Available online at www.sciencedirect.com
ScienceDirect
Journal of Molecular Catalysis A: Chemical 268 (2007) 213–220
JOURNAL OF MOLECULAR CATALYSIS A: CHEMICAL
www.elsevier.com/locate/molcata

Dispersion and site-blocking effect of molybdenum oxide for CO chemisorption on the Pt(1 1 0) substrate

Zhiquan Jiang [a,b], Weixin Huang [b], Hong Zhao [a], Zhen Zhang [a], Dali Tan [a], Xinhe Bao [a,*]

[a] *State Key Laboratory of Catalysis, Dalian Institute of Chemical Physics, Chinese Academy of Sciences, Dalian 116023, China*
[b] *Department of Chemical Physics, University of Science and Technology of China, Hefei 230026, China*

Received 25 August 2006; received in revised form 15 October 2006; accepted 14 December 2006
Available online 20 December 2006

Abstract

The Pt(1 1 0) model surfaces modified by the metallic molybdenum and by the MoOx (molybdenum oxide species) were fabricated via thermal decomposition of $Mo(CO)_6$ and subsequent oxidation on a clean Pt(1 1 0) substrate, by means of Auger electron spectroscopy (AES) and X-ray photoelectron spectroscopy (XPS), as well as high-resolution electron-energy-loss spectroscopy (HREELS). CO chemisorption on these model surfaces was investigated using thermal desorption spectroscopy (TDS) and HREELS. The presence of the metallic molybdenum and MoOx species suppresses CO chemisorption on the Pt(1 1 0) substrate, indicating a physically site-blocking effect. The electron-deficiency of the Pt(1 1 0), due to the modification of metallic molybdenum, causes the low-temperature peak of CO desorption to shift downward in temperature by ∼30 K. The interaction between the MoOx and the underlying Pt(1 1 0) substrate has no influence on CO desorption temperature.

Keywords: Molybdenum; Pt(1 1 0); Thermal desorption spectroscopy; X-ray photoelectron spectroscopy; High-resolution electron-energy-loss spectroscopy

1. Introduction

Molybdenum oxide (MoOx) is one of the most industrially important catalytically active materials useful for a number of oxidative reactions [1,2]. MoOx can also improve the catalytic performance as a promoter or a catalyst support. Supported bimetallic systems containing molybdenum and a group VIII metal, especially platinum, are frequently encountered in the literature. Bimetallic catalysts which consist of Mo and Pt have shown high activity in hydrogenolysis of alkanes [3] and dehydrogenation of cyclohexane [4], while comparable activity was not observed for the monometallic catalysts. The results have been explained by a dual-site mechanism, by which Mo atoms are sites for dissociation of hydrocarbons, while Pt atoms are sites for hydrogenation of carbon or the hydrocarbon fragments. Density functional theory study also suggested that the MoO_3-supported Pt catalyst facilitated single C–H bond activation in CH_4; however, in contrast to the processes on pure metal surfaces, the further dehydrogenation of methyl (CH_3) was very energetically unfavorable [5], suggesting that the Pt/MoO_3 may be an attractive catalyst for the formation of methanol or methanol derivatives. A supported Pt–MoOx–Al_2O_3 system in the fresh and sulfided states, as a desulfurization catalyst, was analyzed for development of analogous systems of HDS process [6]. The incorporation of Mo in the form of MoO_3 to a Pd or Pt catalyst significantly improved not only the performance of the catalyst for the NO conversion with minimal NH_3 formation under reducing conditions, but also the NO conversion under slightly oxidizing conditions [7]. On the molybdenum–platinum bimetallic catalysts supported on alumina, which exhibited high activities in CO hydrogenation than supported monometallic catalysts of Mo or Pt, EXAFS showed equivocally the formation of bimetallic bonds between Mo and Pt; regarding the activities of CO hydrogenation, it was concluded that reduced Mo sites were responsible for the high activity and that Pt helped Mo sites become more reduced [8].

As for electrochemical catalysts, there are several reports about the improvement of CO-tolerance or oxidation activity for CH_3OH on a Pt catalyst by the addition of MoO_3 [9–12]. The mixed-valence oxides of molybdenum, MoOx, have a rutile-type

* Corresponding author at: State Key Laboratory of Catalysis, Dalian Institute of Chemical Physics, Chinese Academy of Sciences, Dalian 116023, China. Tel.: +86 441 84686637; fax: +86 441 84694447.
E-mail address: xhbao@dicp.ac.cn (X. Bao).

1381-1169/$ – see front matter © 2007 Published by Elsevier B.V.
doi:10.1016/j.molcata.2006.12.024

structure with short metal–metal bond distance along the direction of edge sharing, which accounts for the high electronic conductivity of these materials. Besides the metallic conductivity, these MoOx species are relatively stable in acid solution and they have specific catalytic reactivity. On the other hand, dispersion of molybdenum on the MoOx substrate, achieved and enhanced by the metal–support interaction, greatly improves the performance of fuel cells based on platinum electrode. The performance of PEFCs (polymer electrolyte fuel cells) with Pt/MoOx/C was improved under 100 ppm CO-contaminated H_2 conditions compared to the Pt/C catalyst, and was almost comparable to the PtRu(1:1)/C catalyst, the state-of-the-art anode electrocatalyst for PEFC under pure hydrogen fuel conditions [13]. The strong metal–support interaction (SMSI) was regarded as a reasonable explanation for the CO-tolerance of the electrochemical catalysts. The metal–support interaction was also observed between Pt particles and thin film cerium oxide by a significant downward shift in temperature for CO desorption [14]. However, no substantial chemical interaction was detected between the cerium oxide overlayer and the underlying Pt(1 1 1) substrate by X-ray photoemission [15]. On the reduction of NO by H_2 or CO of various PdO–MoO_3/γ-Al_2O_3 catalysts, the interaction between Pd and Mo did not ensure improvements in activity and selectivity, although it was observed even at low MoO_3 content [16,17]. Therefore it is necessary to investigate at the molecular level the promoter effect of metallic molybdenum and molybdenum oxide on the platinum substrate.

Metallic molybdenum deposition on the Pt(1 1 0) surface was achieved via thermal decomposition of $Mo(CO)_6$, and subsequent oxidation converted the surface metallic molybdenum species into the form of molybdenum oxide. CO desorption feature shifts downward in temperature on the Mo/Pt(1 1 0) surface, compared to the clean Pt(1 1 0) substrate, due to the modification of the metallic molybdenum. However, no distinguished shift is observed for CO desorption from the Pt(1 1 0) surface modified by the molybdenum oxide, despite that the interaction may be likely to occur between the MoOx species and the underlying platinum substrate.

2. Experimental

Experiments were carried out in an ultrahigh vacuum (UHV) system with a base pressure of 2.0×10^{-10} mbar, which was described in detail elsewhere [18]. Briefly, the system was equipped with facilities for Auger electron spectroscopy (AES), X-ray photoelectron spectroscopy (XPS), an ELS-22 instrument for high-resolution electron-energy-loss spectroscopy (HREELS), an ion gun for cleaning the sample, and a quadrupole mass analyzer for verification of the purity of the inlet gas and for the thermal desorption spectroscopy (TDS) experiments. A Pt(1 1 0) single crystal was fixed on the sample holder with Ta wires, and the temperature was monitored by a chromel–alumel thermocouple spot-welded on the back side of the sample. In the TDS experiments, the sample was heated at a rate of 8 K/s. In order to avoid the signal except from the front side of the sample, it was positioned at about 3 mm away from the collector of mass spectrometer. The HREEL spectra were taken in the specular direction with an incident angle of 60°, and a primary incident electron beam energy of 5.0 eV. $Mo(CO)_6$, further purified by several freeze-pump-thaw cycles, was fed through a capillary array doser, which was aimed directly at the sample, thus preventing an undesirable rise in the background pressure of $Mo(CO)_6$. The exposure was determined by integrating the pressure increase as a function of dose time, which was measured by an ion gauge without correction. All exposures determined in this way were specified hereafter as Langmuirs ($1\,L = 1.0 \times 10^{-6}$ Torr s).

3. Results and discussion

$Mo(CO)_6$ is usually used as a metal-containing precursor for the preparation of molybdenum species [18,19]. Fig. 1 shows a series of thermal desorption spectra for 28 amu when a clean Pt(1 1 0) surface was exposed to $Mo(CO)_6$. On the clean surface, a desorption peak appears at 520 K, which is assigned to CO adsorbed on Pt(1 1 0) from the background. When the metal substrate is exposed to $Mo(CO)_6$, the peak at 520 K increases in intensity and becomes asymmetric toward lower temperature. This peak is due to thermal decomposition of the adsorbed $Mo(CO)_6$ on Pt(1 1 0), agreeing well with that the desorption intensity increases with $Mo(CO)_6$ exposure. With increasing $Mo(CO)_6$ exposure, an additional peak emerges at 225 K, and gains in intensity continually with $Mo(CO)_6$ exposure, eventually dominating the desorption spectrum. Desorption spectra for $Mo(CO)_6$ from alumina films [18,20], Cu(1 1 1) [21], Rh(1 0 0) [22], Ru(0 0 1) [23] and graphite [24] all demonstrated that $Mo(CO)_6$ did not decompose into metallic molybdenum and evolve CO at temperatures lower than 200 K. Thus, the peak at 225 K can be attributed to molecular desorption of $Mo(CO)_6$ adsorbed on the surface. This 225 K peak shifts upward in desorption temperature with further increasing $Mo(CO)_6$ exposure. The increase in the desorption temperature of this peak with

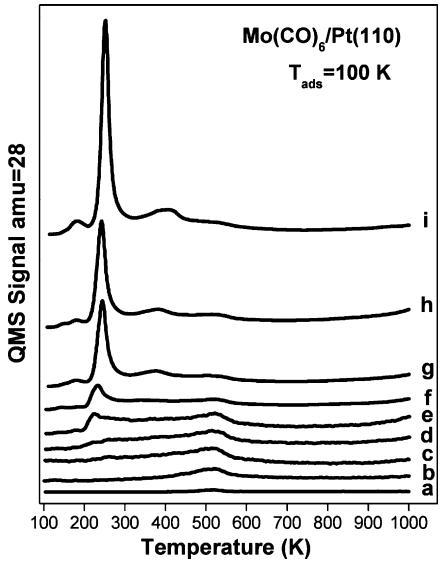

Fig. 1. TDS from the clean Pt(1 1 0) surface with $Mo(CO)_6$ exposure of: (a) 0 L, (b) 0.1 L, (c) 0.2 L, (d) 0.3 L, (e) 0.5 L, (f) 1 L, (g) 3 L, (h) 5 L, and (i) 10 L.

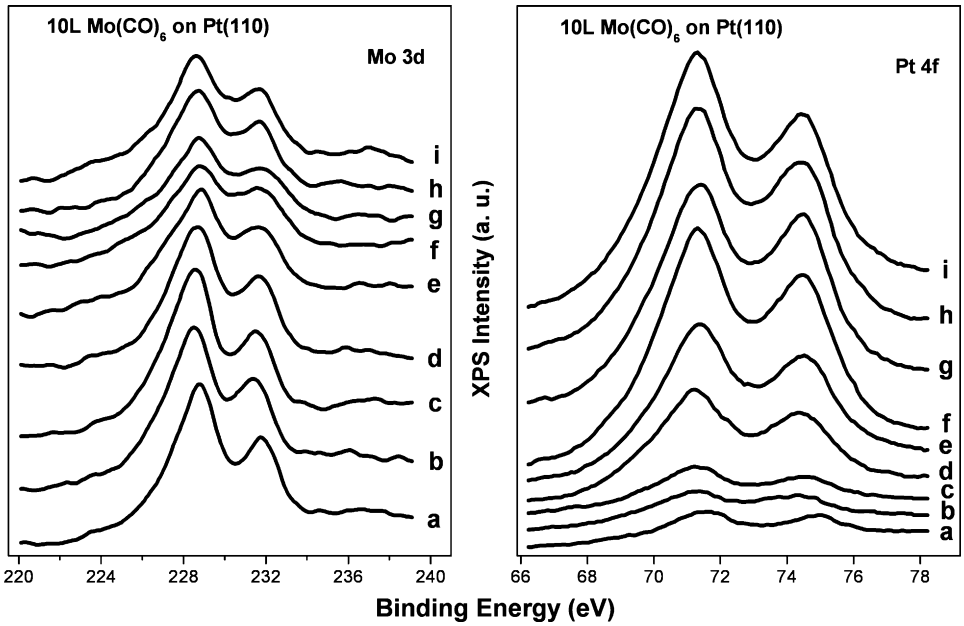

Fig. 2. XPS of Mo 3d and Pt 4f with $Mo(CO)_6$ exposure of 10 L annealed at: (a) 100 K, (b) 150 K, (c) 200 K, (d) 250 K, (e) 300 K, (f) 400 K, (g) 500 K, (h) 600 K, and (i) 700 K on the clean Pt(1 1 0) substrate. The sample was heated slowly to the above temperatures, held for 2 min, cooled down to 100 K.

exposure is a characteristic of zeroth-order kinetics, which was similar to the results reported for $Mo(CO)_6$ on graphite [24] and on Si(1 1 1) -7×7 [25]. This is due to the desorption of $Mo(CO)_6$ multilayers, which can be confirmed by the fact that the intensity continues to increase and does not reach saturation with increasing exposure. Further increasing exposure to $Mo(CO)_6$, the desorption signal exhibits new features at 180 and 405 K. The 180 K peak is also due to the desorption of molecular $Mo(CO)_6$ from Pt(1 1 0). After desorption of most of the adsorbed $Mo(CO)_6$ from the clean Pt(1 1 0) substrate, the residual $Mo(CO)_6$ undergoes thermal decomposition as the substrate temperature increases, so that molybdenum is deposited on the surface. However, the entire process of $Mo(CO)_6$ decomposition is divided into two steps, as indicated by the two separate peaks at 405 and 520 K, respectively. Molybdenum subcarbonyls, intermediate species in thermal decomposition of $Mo(CO)_6$, were detected on alumina [26,27], silica [28] and Rh(1 0 0) [22]. Among the subcarbonyls, $Mo(CO)_3$ (ads) was comparatively stable on the surface [29]. As the temperature increases to 950 K, the desorption signal increases continuously in intensity with heating temperature arising, and also enhances its intensity with increasing $Mo(CO)_6$ exposure. The signal above 900 K is assigned to the recombinative desorption of CO from the surface carbon and oxygen species, which was also found in TPD spectra for an alumina film exposed to 60×10^{-6} Torr s of $Mo(CO)_6$ [30]. Since molybdenum dissociatively adsorbed CO, the surface carbon and oxygen were formed on Pt(1 1 0) during thermal decomposition of $Mo(CO)_6$, as monitored by AES technique.

$Mo(CO)_6$ chemisorption on the clean Pt(1 1 0) surface is further investigated by XPS. Fig. 2 shows Mo 3d and Pt 4f XP spectra taken from the surface annealed at various temperatures after exposure to 10 L $Mo(CO)_6$ at 100 K. The Mo 3d doublet appears at 228.8 and 231.8 eV, corresponding to physically adsorbed layers of $Mo(CO)_6$. This was also observed on a polycrystalline Cu surface [31], where the Mo 3d peaks appeared with binding energies of 228.9 and 232.1 eV at 109 K. As the substrate temperature increases, the adsorbates decompose and the molybdenum subcarbonyl species form, hence the Mo 3d doublet shifts towards lower binding energy and decreases its intensity to some extent. Cho and Bernasek [32] also observed similar phenomena when they used wide-band UV radiation from a mercury lamp to irradiate the adsorbed $Mo(CO)_6$ layers, since $Mo(CO)_6$ underwent partial decomposition under UV radiation. Further increasing substrate temperature results in complete decomposition of molybdenum subcarbonyl species and deposition of molybdenum on the oxide surface. At 700 K, the Mo 3d peaks settle at 228.6 and 231.6 eV. When the Pt(1 1 0) substrate was exposed to $Mo(CO)_6$, the thick adsorption layer hinders the photoemission of the underlying platinum, drastically decreasing the Pt 4f XPS intensity. With increasing sample temperature, Pt 4f XPS signal grows in intensity, due to desorption of the thick adsorption layer.

It can be deduced from the above results that $Mo(CO)_6$ decomposes completely and Mo is left on the platinum surface at a substrate temperature of 600–700 K. The HREELS results (not shown) of $Mo(CO)_6$ chemisorption on the Pt(1 1 0) surface at 100 K and subsequent annealing process also suggest that entire decomposition of $Mo(CO)_6$ occurs at the sample temperature of 600 K. Both desorption and decomposition reactions occur during heating, in which the heating rate plays a very important role on the ratio between desorption and decomposition of the adsorbed $Mo(CO)_6$ species. In most cases, the desorption reaction overwhelms the decomposition reaction. It was reported that slow heating would leave a significant amount of Mo on the surface, while rapid heating (5–10 K/s) could reduce this amount to about only one-tenth, when $Mo(CO)_6$ was used as a metal-containing precursor [31,32]. The heating rate in the TDS measurements is far higher than that in the XPS mea-

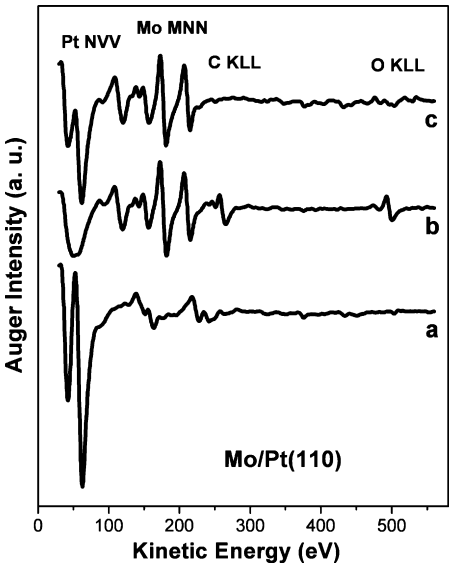

Fig. 3. AES of the model surfaces: (a) clean Pt(1 1 0) substrate, (b) molybdenum deposition onto Pt(1 1 0) at 700 K, and (c) the Mo/Pt(1 1 0) surface annealed at 1000 K. The deposited molybdenum coverage was estimated at ∼2 ML.

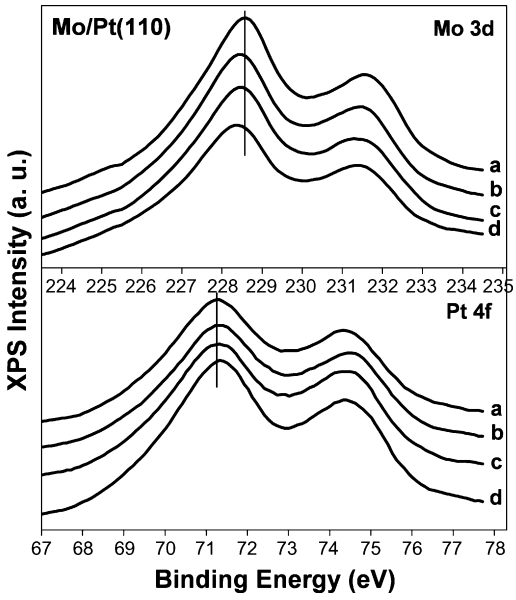

Fig. 4. XPS of Mo 3d and Pt 4f with molybdenum coverage of ∼2 ML deposited at 700 K on the clean Pt(1 1 0) substrate, then annealed at: (a) 700 K; (b) 800 K; (c) 900 K; (d) 1000 K for 2 min.

surements, therefore a large amount of $Mo(CO)_6$ desorbs from the surface when it is heated to 250 K in the TDS experiments. However, the Mo 3d XPS intensity does not decrease so drastically in the XPS measurements, as shown in Fig. 2. No obvious change of the HREELS (not shown) is likewise observed on the $Mo(CO)_6$/Pt(1 1 0) sample at 250 K, as compared to that at 100 K. After molybdenum deposition via thermal decomposition of $Mo(CO)_6$, some C and O contaminants exist in the deposited layer, as confirmed by AES and XPS. These contaminants are the results of the dissociation of CO, catalyzed by the metallic molybdenum present on the surface [31,33,34]. Upon heating the sample to 1000 K, the C and O contaminants recombine and evolve CO from the surface. Fig. 3 shows AES during this process of molybdenum deposition onto the clean Pt(1 1 0) surface, where the C and O contaminants emerge after molybdenum deposition at 700 K and disappear after annealed at 1000 K. Hence a Pt(1 1 0) surface modified by the metallic molybdenum was obtained, without any C and O contaminants derived from thermal decomposition of $Mo(CO)_6$.

Fig. 4 shows a series of the Mo 3d and Pt 4f XP spectra taken from the surface heated to the indicated temperatures after molybdenum deposition at 700 K under a $Mo(CO)_6$ pressure of 4.5×10^{-8} mbar for 30 min. The amount of molybdenum deposit is estimated to be ∼2 ML from the attenuation of the Pt 4f core level and from photoelectron emission from the deposited molybdenum. The Mo $3d_{5/2}$ peak appears with a binding energy of 228.6 eV at 700 K. Increasing the sample temperature causes the Mo 3d doublet to shift downward in binding energy, with a Mo $3d_{5/2}$ value of 228.4 eV at 1000 K. Pt 4f doublet has no observable binding energy shift during the annealing process, only a slight tendency of upward shift. No obvious change of the Pt 4f XPS signal is probably due to the massive substrate effect. We observed this substrate effect on the Sm/Rh(1 0 0) system, where ∼2 ML Sm was deposited onto a clean Rh(1 0 0) surface [35]. Similar phenomena were also observed on the Cu/Rh(1 0 0) and Cu/Ru(0 0 0 1) systems, where no change in line shape or in the separation between the Rh 3d and Ru 3d peaks, but only corresponding decreases in Rh and Ru intensities with increasing Cu coverage were observed [22]. No prominent change for the Pt 4f doublet may also be due to little shift in binding energy, for a lack of resolution in standard XPS. The distinct downward shift in binding energy of the Mo 3d doublet indicates that electron transfer occurs from the underlying platinum substrate to the deposited molybdenum, inducing the adjacent platinum electron-deficient. This electron-deficiency of the platinum substrate would have an impact on the adsorption property of adsorbates on the Mo-modified Pt(1 1 0) surface.

On the Pt(1 1 0) surface modified by the metallic molybdenum, CO thermal desorption was performed with various exposures at room temperature, as shown in Fig. 5. When CO exposure is low, a desorption signal appears at 420 K. With increasing exposure to CO, this desorption peak gains in intensity and shift downward in temperature, settling at 397 K with CO exposure of 0.5 L. An additional signal emerges at 503 K as a shoulder at higher temperature with CO exposure of 0.5 L, and it continues to intensify with further increasing CO exposure. At the same time, the low-temperature peak holds constant in desorption temperature, which settles at ∼389 K with CO exposure higher than 2 L; the desorption intensity keeps on growing, eventually approaches to saturation with CO exposure of 10 L. However, CO desorption from the Mo/Pt(1 1 0) surface is different from that from a clean Pt(1 1 0) surface. When low exposure of CO was dosed on Pt(1 1 0), a desorption signal appeared at 510 K; with increasing CO exposure, another peak emerged at 380 K, accompanied with the increased intensity of CO desorption signal at 510 K [36]. The second signal, derived with the increase of CO coverage on the Pt(1 1 0) surface, was explained by the mutual repulsion among the adsorbed CO molecules. Whereas, in our case, CO desorption preferentially exhibits a

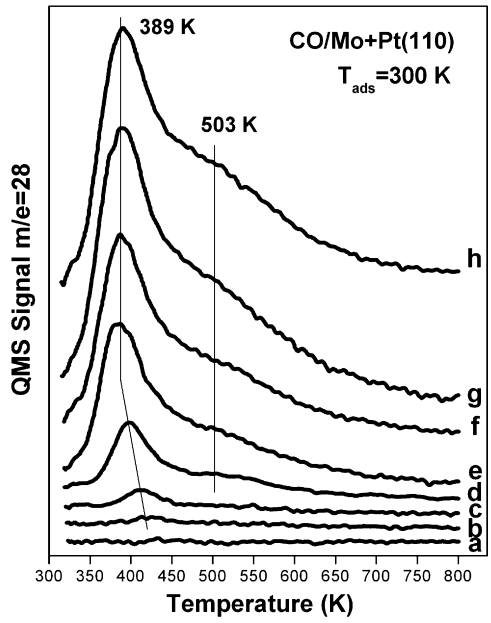

Fig. 5. Thermal desorption spectra of CO on the Pt(1 1 0) surface precovered by ~2 ML metallic molybdenum. CO was dosed on the model surface at room temperature with exposure of: (a) 0 L, (b) 0.1 L, (c) 0.2 L, (d) 0.5 L, (e) 2 L, (f) 5 L, (g) 10 L, (h) 15 L.

low-temperature signal at low exposure on the Mo/Pt(1 1 0) surface.

The Mo/Pt(1 1 0) surface was obtained by annealing at 1000 K after molybdenum deposition onto Pt(1 1 0) surface via thermal decomposition of $Mo(CO)_6$, as evidenced by AES and XPS. Then this model surface was oxidized for 30 min in 5.0×10^{-6} mbar of O_2, and the Pt(1 1 0) surface modified by the molybdenum oxide was formed. Fig. 6 shows HREELS and AES during oxidation process of the Mo/Pt(1 1 0) surface with nominal molybdenum coverage of ~2 ML. After oxidation at 700 K, the oxygen signal is present on the surface, as monitored by AES. Three vibrational peaks appear in HREEL spectrum at 540, 700 and 1000 cm^{-1} on the oxidized Mo/Pt(1 1 0) surface, where the feature is similar to the case of oxygen adsorption on Mo(1 1 0) [37–39], Mo(1 0 0) [40,41], Mo(1 1 1) [42] and Mo(1 1 2) [43] surfaces. The former two peaks are assigned to Mo–O deformation and stretching mode, respectively, while the latest peak is attributed to the stretching mode of terminal atop oxygen on the topmost Mo atoms. The conclusive assignment of the peak at 1000 cm^{-1} to the Mo=O moiety, is deduced not only from HREELS studies of oxidized Mo(1 1 0) [37,38], but also from HREELS study of MoO_3 [44] and comparison to other investigations of molybdenum oxide, including infrared [45,46] and Raman studies [47,48] of model catalysts systems containing MoO_3. Upon heating the oxidized surface to higher temperatures, the former two peaks evolve into one feature at 600 cm^{-1}, which increases in intensity with the sample temperature, while the signal at 1000 cm^{-1} loses its intensity and eventually disappears after 1000 K annealing. The peak at 600 cm^{-1} is attributed to the symmetric stretching mode of the Mo–O–Mo bridge bond, which is deduced from the Raman vibration of the bulk MoO_3 [48,49]. The disappearance of the signal due to terminal Mo=O species upon heating was also observed on the oxidized Mo(1 1 0) substrate, where the Mo=O sites were subsequently depopulated by heating at high temperatures, indicating the absence of terminal oxygen species [50]. This may be explained by that annealing at high temperatures causes the oxygen to migrate into the bulk, and bring molybdenum into high oxidation state. It is supported by the emergence of the Mo–O–Mo bridge bond, also by the appearance of the feature between 1500 and 2000 cm^{-1} after annealing at 1000 K, which is due to the combinative and multiple phonon losses of the low-frequency peaks. This suggests that an intermediate molyb-

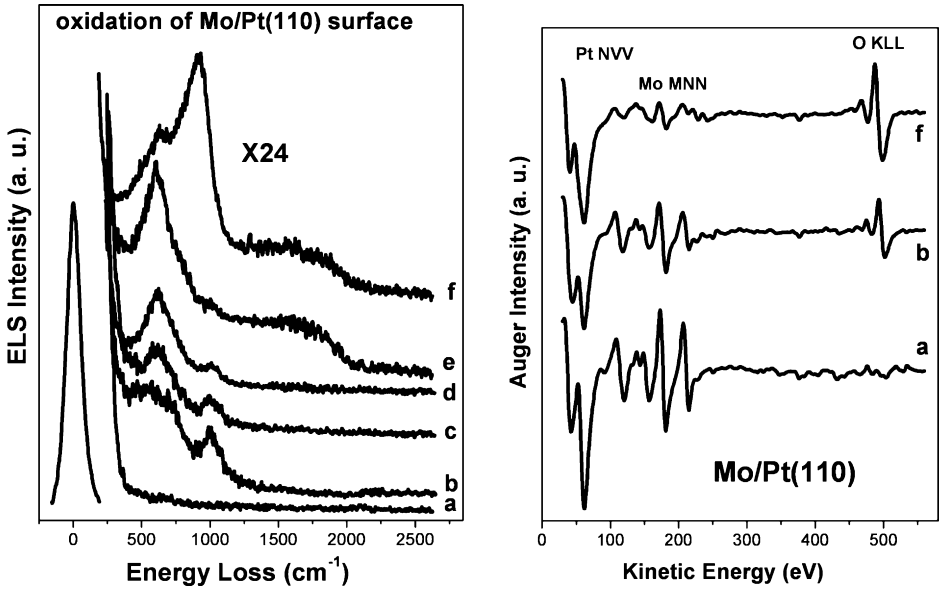

Fig. 6. Spectral features of the Mo/Pt(1 1 0) surface during high-temperature oxidation: (a) the Mo/Pt(1 1 0) surface with molybdenum coverage of ~2 ML; after oxidation at 700 K for 30 min in 5.0×10^{-6} mbar O_2, annealed at (b) 700 K, (c) 800 K, (d) 900 K, (e) 1000 K; (f) oxidation at 1000 K for 30 min in 5.0×10^{-6} mbar O_2.

denum oxide species has been formed on the Pt(1 1 0) surface. In an attempt to obtain much heavier oxidation of molybdenum, the Mo/Pt(1 1 0) surface was oxidized at 1000 K for 30 min in 5.0×10^{-6} mbar of oxygen. Besides the vibrational signal at 620 cm^{-1}, a stronger peak appears at 920 cm^{-1}, indicating that the molybdenum is in a heavy oxidation state. The presence of this oxidative state of the surface molybdenum species is also suggested by the difference of the signals (e) and (f) in the left panel, which are due to the terminal Mo=O species. The formation of molybdenum oxide upon high-temperature oxidation was also observed on the Mo(1 1 0) surface, as confirmed by the appearance in the HREEL spectra of a feature at ~1000 cm^{-1} associated with the Mo=O moiety [38]. However, many of the molybdenum species are lost from the model surface during high-temperature oxidation, as indicated by AES in the right panel of Fig. 6, since molybdenum oxide is volatile compared to the metallic molybdenum. From the AES peak-to-peak intensity of curve (f) in the right panel, the molar ratio of Mo to O is estimated to be 0.393, close to the stoichiometry of the bulk MoO_3. To avoid the loss of more of the surface molybdenum species, we did not oxidize the model surface under more rigorous conditions. Then the surface by oxidation at 1000 K in 5.0×10^{-6} mbar of O_2 was denoted as the MoOx/Pt(1 1 0).

Fig. 7 shows a series of TDS for 28 amu when the MoOx/Pt(1 1 0) surface was exposed to CO at room temperature. Dosing CO to the MoOx/Pt(1 1 0) surface causes a desorption signal to emerge at 505 K. Another desorption signal appears at 420 K with CO exposure of 0.5 L. These two peaks both intensify along with CO exposure, and their features hold substantially constant in desorption temperature. There was negligible adsorption of CO on MoO_3 under UHV conditions following dehydroxylation at 1200 K and dosing with an equilibrium pressure of 5.0 Torr of CO at 140 K probed by IR spectra [51]. The surface molybdenum species is stoichiometrically close to MoO_3, as indicated by AES in the right panel of Fig. 6. Therefore this surface MoOx species needs not to be taken into consideration for CO chemisorption at room temperature. CO desorption from the MoOx/Pt(1 1 0) surface, entire contribution from the underlying platinum substrate, is much weaker than that from the clean Pt(1 1 0) surface. The weakness of CO desorption is due to a simple site-blocking of the surface MoOx, which spreads over the Pt(1 1 0) surface upon annealing. In earlier experiments an almost unrestricted spreading of the supported molybdates uncovered only undetectably small parts of the support surface [52,53]. Again laser Raman spectroscopy investigation [54] and IR and TPD measurements [51] of MoO_3/Al_2O_3 catalysts indicated that under dehydrating conditions polymeric molybdate species spread to form octahedrally coordinated MoO_3 units on the surface of γ-Al_2O_3. In recent studies on silica support [48] and on alumina model supports [55,56] spreading of MoO_3 was also observed: after thermal treatment, MoO_3 formed a monolayer or a submonolayer on the flat surface of the stable Al_2O_3 and SiO_2 thin films. The spreading of the surface MoOx blocks some adsorption sites on the Pt(1 1 0) and suppresses CO chemisorption, indicating the prominent site-blocking effect. The site-blocking effect for CO chemisorption was also observed on zirconium oxide deposited on the Pt(0 0 1) substrate [57].

For comparison, CO desorption spectra with 15 L exposure from the clean Pt(1 1 0), Mo/Pt(1 1 0) and MoOx/Pt(1 1 0) surfaces, on which the desorption intensities sequentially decreases, are listed in Fig. 8. The attenuation of the desorption intensity is due to the site-blocking effect of the surface molybdenum and MoOx, which occupy adsorption sites for CO and suppress CO chemisorption. The high-temperature component holds constant in desorption temperature on the three model surfaces, substan-

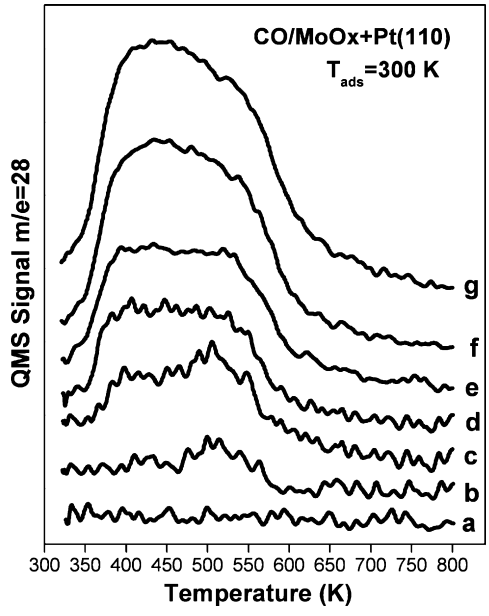

Fig. 7. Thermal desorption spectra from the MoOx/Pt(1 1 0) surface with CO exposure of: (a) 0 L, (b) 0.2 L, (c) 0.5 L, (d) 2 L, (e) 5 L, (f) 10 L, and (g) 15 L at room temperature.

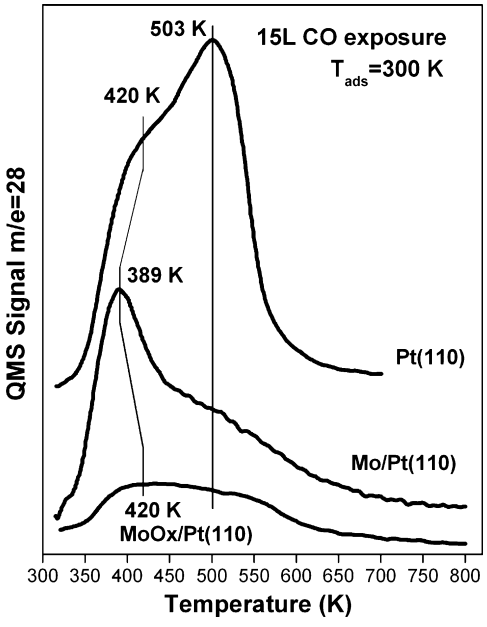

Fig. 8. Thermal desorption spectra of CO on: (a) the clean Pt(1 1 0) substrate, (b) the Mo/Pt(1 1 0) and (c) the MoOx/Pt(1 1 0) surfaces. 15.0 L CO was dosed on the model surfaces at room temperature.

tially at 503 K with CO exposure of 15 L. The low-temperature one shifts downward by ~30 K on the Mo/Pt(1 1 0) surface compared to that on the clean Pt(1 1 0) substrate, while it restores on the MoOx/Pt(1 1 0) surface. As mentioned above, the electron-deficiency of the platinum substrate is due to the modification of metallic molybdenum. Thus it weakens the electron backdonation from platinum substrate to the adsorbed CO, inducing CO desorption at lower temperature. The downward shift in temperature of CO desorption from a Pt/CeOx film, compared to CO adsorbed on a Pt single crystal, was ascribed to a weakening of the CO–Pt bond that resulted from an electronic interaction between the Pt and the reduced ceria [14]. High-temperature oxidation causes the molybdenum species to form oxide islands on the MoOx/Pt(1 1 0) surface, since it is easy for molybdenum oxide to migrate and aggregate. However, no obvious difference for CO desorption is observed on the Pt(1 1 0) substrate and on the MoOx/Pt(1 1 0) surface, besides that the intensity of the former is much larger than that of the latter. This indicates that no interaction exists between the MoOx and the underlying platinum substrate. Another more reasonable explanation is that a very weak interaction exists between the MoOx and the Pt(1 1 0), but this interaction do not have any influence on CO desorption, as observed on PdO–MoO_3/γ-Al_2O_3 catalysts [16,17].

Fig. 9 shows a series of HREELS annealed at the indicated temperatures of the Pt(1 1 0) substrate (upper) and the Mo/Pt(1 1 0) surface (bottom) with 15 L CO dosed at room temperature. Due to the interference of the strong phonon losses, HREELS for CO chemisorption on the MoOx/Pt(1 1 0) was not obtained. When CO was dosed at room temperature, the peak for M–CO stretching mode appears at 471 cm^{-1} and the peak for C–O stretching mode at 2120 cm^{-1} on the clean Pt(1 1 0), while the corresponding peaks emerge at 415 and 2089 cm^{-1}

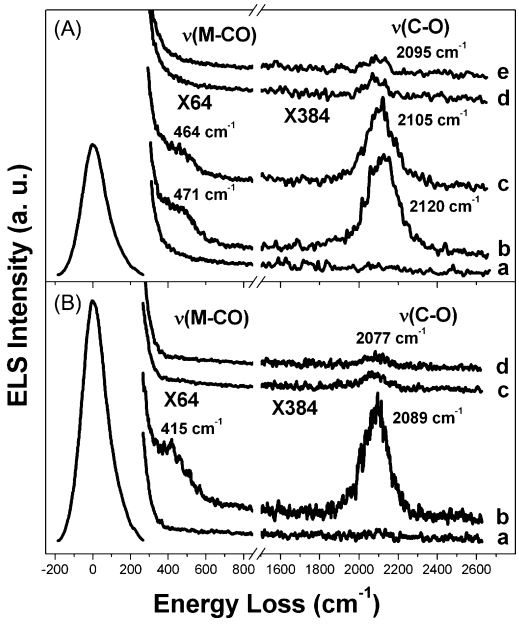

Fig. 9. HREELS of the Pt(1 1 0) substrate (upper) and the Mo/Pt(1 1 0) surface (bottom) with 15.0 L CO dosed at room temperature. (a) The clean Pt(1 1 0) substrate and the Mo/Pt(1 1 0) surface, respectively; after dose of 15.0 L CO at room temperature, annealed at (b) 300 K, (c) 400 K, (d) 500 K, (e) 600 K.

on the Mo/Pt(1 1 0) surface, respectively. The appearance of the vibrational features, M–CO stretching mode at low frequency and C–O stretching mode at high frequency, indicates molecular adsorption of CO on the Pt(1 1 0) and Mo/Pt(1 1 0) surfaces. The C–O stretching vibration exhibits one single feature on the two model surfaces, indicating that only one kind of adsorbed species appears upon CO dose. This is in accordance with the results in literature [58], where CO chemisorption exhibited one loss signal on the Pt(1 1 0) surface, while two separate peaks on the Pt(1 1 1) substrate. Neither bridge bonded CO nor any other adsorption site were detected on the Pt(1 1 0), independent of CO coverage, in good agreement with Sharma et al. who reported that CO occupied top sites on Pt(1 1 0) at all coverages and temperatures from 90 to 300 K [59]. However, two distinguished features are observed on CO TDS from the Pt(1 1 0) substrate with 15 L CO dose at room temperature. This is explained by mutual repulsion among the adsorbed molecules [36]. The M–CO stretching frequency on the Pt(1 1 0) is higher than that on the Mo/Pt(1 1 0) surface, suggesting that CO bonds the former stronger than the latter. The difference of the M–CO stretching frequency on these two model surfaces is probably due to the discrepancy in electron backdonation from the substrate to the adsorbed CO. A stronger strength of CO bonding results in a higher desorption temperature in the TDS. Therefore the low-temperature component on the Mo/Pt(1 1 0) surface is observed to shift downward by ~30 K, as compared to that on the Pt(1 1 0). The M–CO stretching mode disappears on the Mo/Pt(1 1 0) surface upon 400 K annealing, only a weak C–O stretching signal is still visible in the HREEL spectrum; while the M–CO and C–O stretching modes on the Pt(1 1 0) substrate are discernible upon 400 K annealing, and undetectable upon 500 K annealing. The disappearance sequence of the M–CO and C–O stretching modes on the Pt(1 1 0) and Mo/Pt(1 1 0) surfaces upon annealing is in good agreement with the TDS results of CO. Upon annealing the samples at 400 K, a small amount of the adsorbed CO is rudimental on the Mo/Pt(1 1 0) surface, while most of the adsorbed CO still stays on the Pt(1 1 0) substrate, as indicated in Fig. 8.

4. Conclusions

Molybdenum deposition on Pt(1 1 0) was achieved via thermal decomposition of $Mo(CO)_6$ at 700 K, and subsequent annealing at 1000 K gave a model surface of Pt(1 1 0) modified by the metallic molybdenum, without any carbon and oxygen contaminants. The MoOx/Pt(1 1 0) surface, as evidenced by the vibrational features at 620 and 920 cm^{-1} and the broad loss signal between 1500 and 2000 cm^{-1}, was fabricated by oxidation of the Mo/Pt(1 1 0) surface at 1000 K. CO thermal desorption from these model surfaces at room temperature was investigated, to monitor the discrepancy of adsorption sites due to modification by the metallic molybdenum and by the MoOx. The desorption intensities decrease in the sequence of the clean Pt(1 1 0), Mo/Pt(1 1 0) and MoOx/Pt(1 1 0) surfaces, indicating a physically site-blocking effect. The high-temperature components remain constant in temperature, while the low-temperature one shifts downward by ~30 K on the Mo/Pt(1 1 0) surface com-

pared to that on the clean Pt(1 1 0) substrate, and restores on the MoOx/Pt(1 1 0) surface. The downward shift in temperature is indicative of the electron-deficiency of the Pt(1 1 0) substrate, which is due to modification of the metallic molybdenum. The weak interaction, occurring between the molybdenum oxide species and the underlying Pt(1 1 0) substrate, has no influence on CO desorption temperature, besides a physically site-blocking effect.

Acknowledgement

This work was financially supported by the National Natural Science Foundation of China (90206036).

References

[1] U. Ozkan, G.L. Schrader, J. Catal. 95 (1985) 120.
[2] Y.D. Tong, J.H. Lunsford, J. Am. Chem. Soc. 113 (1991) 4741.
[3] T.M. Tri, J. Massardier, P. Gallezot, B. Imelik, J. Catal. 85 (1984) 244.
[4] G. Leclercq, T. Romero, S. Pietrzyk, J. Grimblot, L. Leclercq, J. Mol. Catal. 25 (1984) 67.
[5] C.J. Zhang, P. Hu, J. Chem. Phys. 116 (2002) 4281.
[6] Z. Paál, P. Tétényi, M. Muhler, U. Wild, J.-M. Manoli, C. Potvin, J. Chem. Soc. Faraday Trans. 94 (1998) 459.
[7] B. Frank, R. Lübke, G. Emig, A. Renken, Chem. Eng. Technol. 21 (1998) 498.
[8] S.H. Choi, J.S. Lee, J. Catal. 167 (1997) 364.
[9] H.Q. Zhang, Y. Wang, E.R. Fachini, C.R. Cabrera, Electrochem. Solid-State Lett. 2 (1999) 437.
[10] Y. Wang, E.R. Fachini, G. Cruz, Y.M. Zhu, Y. Ishikawa, J.A. Colucci, C.R. Cabrera, J. Electrochem. Soc. 148 (2001) C222.
[11] E.M. Crabb, M.K. Ravikumar, Y. Qian, A.E. Russell, S. Maniguet, J. Yao, D. Thompsett, M. Hurford, S.C. Ball, Electrochem. Solid-State Lett. 5 (2002) A5.
[12] L.C. Ordóñez, P. Roquero, P.J. Sebastian, J. Ramírez, Catal. Today 107/108 (2005) 46.
[13] T. Ioroi, N. Fujiwara, Z. Siroma, K. Yasuda, Y. Miyazaki, Electrochem. Commun. 4 (2002) 442.
[14] D.R. Mullins, K.Z. Zhang, Surf. Sci. 513 (2002) 163.
[15] K.-D. Schierbaum, Surf. Sci. 399 (1998) 29.
[16] I. Halasz, A. Brenner, M. Shelef, Catal. Lett. 16 (1992) 311.
[17] I. Halasz, A. Brenner, M. Shelef, Catal. Lett. 18 (1993) 289.
[18] Z.Q. Jiang, W.X. Huang, J. Jiao, H. Zhao, D.L. Tan, R.S. Zhai, X.H. Bao, Appl. Surf. Sci. 229 (2004) 43.
[19] R.-I. Nakamura, R.G. Bowman, R.L. Burwell, J. Am. Chem. Soc. 103 (1981) 673.
[20] M. Kaltchev, W.T. Tysoe, J. Catal. 193 (2000) 29.
[21] Z.C. Ying, W. Ho, J. Chem. Phys. 93 (1990) 9077.
[22] T.A. Germer, W. Ho, J. Vac. Sci. Technol. A 7 (1989) 1878.
[23] H.H. Huang, C.S. Sreekanth, C.S. Seet, X. Jiang, G.Q. Xu, Surf. Sci. 365 (1996) 769.
[24] S.K. So, W. Ho, J. Chem. Phys. 95 (1991) 656.
[25] N.S. Gluck, Z. Ying, C.E. Bartosch, W. Ho, J. Chem. Phys. 86 (1986) 4957.
[26] A. Brenner, R.L. Burwell, J. Am. Chem. Soc. 97 (1975) 2565.
[27] K.P. Reddy, T.L. Brown, J. Am. Chem. Soc. 117 (1995) 2845.
[28] M. Kurhinen, T. Venäläinen, T.A. Pakkanen, J. Phys. Chem. 98 (1994) 10237.
[29] C.C. Williams, J.G. Ekerdt, J. Phys. Chem. 97 (1993) 6843.
[30] M. Kaltchev, W.T. Tysoe, J. Catal. 196 (2000) 40.
[31] C.C. Cho, S.L. Bernasek, J. Appl. Phys. 65 (1989) 3035.
[32] C.C. Cho, S.L. Bernasek, J. Vac. Sci. Technol. A 5 (1987) 1088.
[33] R. Solanski, P.K. Boyer, J.E. Mahan, G.J. Collins, Appl. Phys. Lett. 38 (1981) 572.
[34] D.K. Flynn, J.I. Steinfeld, J. Appl. Phys. 59 (1986) 3914.
[35] Z.Q. Jiang, W.P. Zhou, D.L. Tan, R.S. Zhai, X.H. Bao, Surf. Sci. 565 (2004) 269.
[36] P. Hofmann, S.R. Bare, D.A. King, Surf. Sci. 117 (1982) 245.
[37] M.L. Colaianni, J.G. Chen, W.H. Weinberg, J.T. Yates, Surf. Sci. 279 (1992) 211.
[38] S.C. Street, G. Liu, D.W. Goodman, Surf. Sci. 385 (1997) L971.
[39] C.M. Friend, K.T. Queeney, D.A. Chen, Appl. Surf. Sci. 142 (1999) 99.
[40] B.R. Parker, J.F. Jenkins, P.C. Stair, Surf. Sci. 372 (1997) 185.
[41] S.H. Kim, P.C. Stair, J. Phys. Chem. B 104 (2000) 3035.
[42] P.K. Stefanov, Ts.S. Marinova, Surf. Sci. 200 (1988) 26.
[43] T. Sasaki, Y. Goto, R. Tero, K.-I. Fukui, Y. Iwasawa, Surf. Sci. 502/503 (2002) 136.
[44] S.C. Street, D.W. Goodman, J. Vac. Sci. Technol. A 15 (1997) 1717.
[45] T. Wadayama, T. Saito, W. Suëtaka, Appl. Surf. Sci. 20 (1984) 199.
[46] Y. Iwasawa, Y. Nakano, S. Ogasawara, J. Chem. Soc. Faraday Trans. I 74 (1978) 2986.
[47] B.M. Weckhuysen, J.-M. Jehng, I.E. Wachs, J. Phys. Chem. B 104 (2000) 7382.
[48] S. Braun, L.G. Appel, V.L. Camorim, M. Schmal, J. Phys. Chem. B 104 (2000) 6584.
[49] G. Mestl, T.K.K. Srinivasan, Catal. Rev. Sci. Eng. 40 (1998) 451.
[50] K.T. Queeney, C.M. Friend, J. Chem. Phys. 109 (1998) 6067.
[51] A.L. Diaz, M.E. Bussell, J. Phys. Chem. 97 (1993) 470.
[52] M.I. Zaki, B. Vielhaber, H. Knözinger, J. Phys. Chem. 90 (1986) 3176.
[53] J. Leyrer, B. Vielhaber, M.I. Zaki, S. Zhuang, J. Weitkamp, H. Knözinger, Mater. Chem. Phys. 13 (1985) 301.
[54] C.C. Williams, J.G. Ekerdt, J.-M. Jehng, F.D. Hardcastle, I.E. Wachs, J. Phys. Chem. 95 (1991) 8791.
[55] S. Günther, M. Marsi, A. Kolmakov, M. Kiskinova, M. Noeske, E. Taglauer, G. Mestl, U.A. Schubert, H. Knözinger, J. Phys. Chem. B 101 (1997) 10004.
[56] G. Mestl, H. Knözinger, Langmuir 14 (1998) 3964.
[57] U. Bardi, P.N. Ross, Langmuir 9 (1993) 132.
[58] H. von Schenck, E. Janin, O. Tjernberg, M. Svensson, M. Göthelid, Surf. Sci. 526 (2003) 184.
[59] R.K. Sharma, W.A. Brown, D.A. King, Surf. Sci. 414 (1998) 68.